Phonon Speed, Not Scattering, Differentiates Thermal Transport in Lead Halide Perovskites

Giselle A. Elbaz[1], Wee-Liat Ong[1,2], Evan A. Doud[1], Philip Kim[3], Daniel W. Paley*[1], Xavier Roy*[1], Jonathan A. Malen*[2]*

[1]Department of Chemistry, Columbia University, New York, New York 10027.

[2]Department of Mechanical Engineering, Carnegie Mellon University, Pittsburgh, Pennsylvania 15213.

[3]Department of Physics, Harvard University, Cambridge, Massachusetts, 02138

* Email: jonmalen@andrew.cmu.edu, xr2114@columbia.edu, dwp2111@columbia.edu, wlo2103@columbia.edu

Supplementary Information:

I. Synthesis

All perovskite single crystals were grown by vapor diffusion as previously described for $MAPbCl_3$, $MAPbI_3$ and $APbBr_3$ (A = MA, FA, Cs) in Ref. 1, 2, and 3 respectively.

II. FDTR fitting parameters

To extract *k* from the FDTR, the parameters in Table S1 were used. The focused laser spot radius was allowed to vary 3.1 ± 0.1 μm from the measured value during fitting in order to get a better fit on the data. This range is within the measurement uncertainty of the spot radius, which is 4 % of the spot radius.

Table S.1: Fitting parameters for FDTR

	Layer Thickness	**Thermal Conductivity (W/m-K)**	**Volumetric Heat Capacity (kJ/m^3-K)**
Au	60 - 70 nm (measured by AFM)	Measure using 4-point probe method and calculate k_{Au} from Weidemann-Franz Law	2500 (@ 300 K, otherwise use Ref. 4)
Perovskite crystal	>100 μm (estimated from top view of microscopic images)	Fitting parameter from FDTR	Measured by DSC or from Ref. 5.
Substrate	No effect on the fitted *k*	No effect on the fitted *k*	No effect on the fitted *k*

III. Heat Capacity Measurements of $CsPbBr_3$ and $FAPbBr_3$

The heat capacity must be known for our fitting of the FDTR data to extract *k*. While this has been previously reported for the $MAPbX_3$ series,[5] it has not been for $CsPbBr_3$ and $FAPbBr_3$. We therefore performed differential scanning calorimetry (DSC) on samples of $CsPbBr_3$ and $FAPbBr_3$. The DSC was performed using a TA Instrument Q20. Scans were run with 8–15 mg of the respective perovskite crystals sealed hermetically in Tzero aluminium pans. The heating and cooling DSC cycles were performed from 190 to 323 K at rates of either 10 or 20 K min^{-1} with an isothermal interval of five minutes between heating and cooling runs. The measured heat capacity for a piece of 7.1 mg reference Si crystal was within 3% of the published result over the entire temperature range. Uncertainty in the heat capacity of these samples is about 7%, coming from the maximum variation across three separate measurements. The dotted line represents our linearly extrapolated estimates.

$FAPbBr_3$ shows a first-order phase transition at about 265 K corresponding to the previously reported primitive cubic to body-centered cubic phase transition.

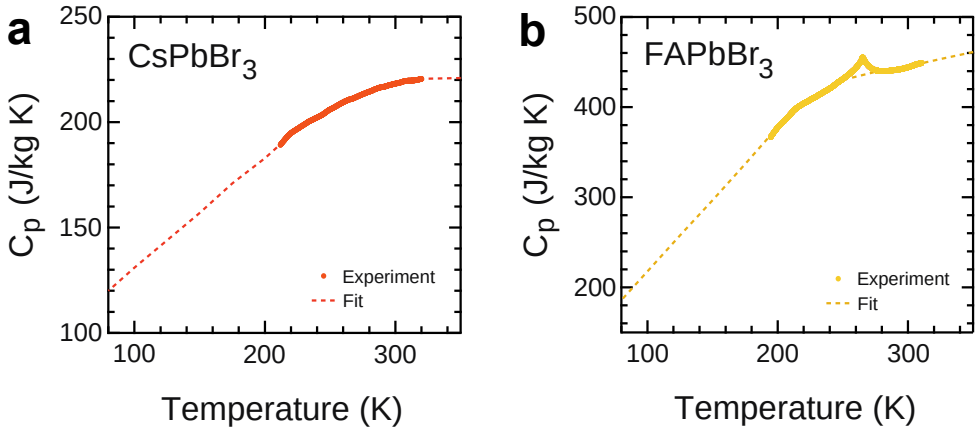

Figure S1: Experimental heat capacities of (a) $CsPbBr_3$ and (b) $FAPbBr_3$. The dotted line represents our linearly extrapolated estimates to lower temperatures.

IV. Nanoindentation

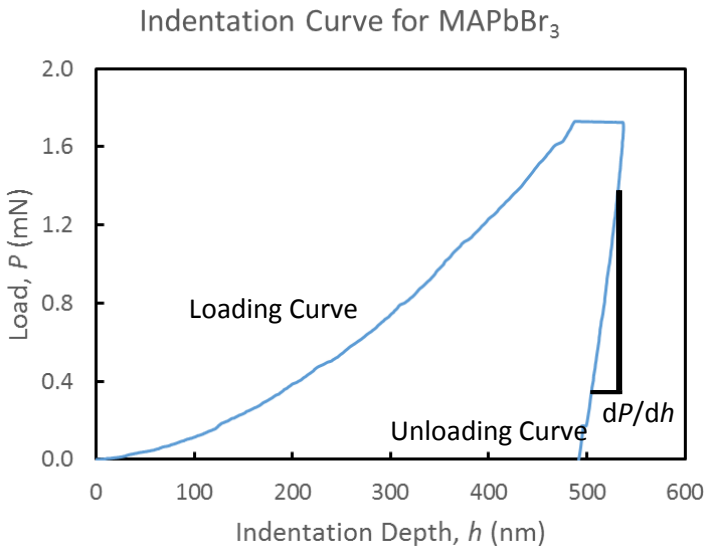

Figure S2: Representative nanoindentation curves for the loading and unloading of an indent on a $MAPbBr_3$ crystal.

The group velocity of acoustic phonons can be approximated as sound speed (v_s) in the material, which we estimate from the density, ρ, and elastic modulus, E, for each of the perovskites. While density is easily calculated from SCXRD, the elastic modulus must be measured separately. To do so, we use a technique known as nanoindentation, which measures the indentation load, P, at a given penetration depth, h, into the surface. We used an MTS Nanoindenter XP on three separate crystals on which at least six indents was performed to determine the elastic modulus, E. Penetration depths of 500 and 1000 nm were used on all crystals with no significant variation seen in the resulting elastic modulus. Each indentation was then unloaded from its penetration depth, and E was calculated using the slope of the unloading curve as shown in Figure S2 for a typical gold-coated $MAPbBr_3$ single crystal.

To calculate the elastic modulus, E, the slope of the unloading curve, which is shown as dP/dh, is taken to be the unloading stiffness, S. This stiffness is related to the effective elastic modulus (E_f) through equation (S1),

$$S = \beta \frac{2}{\sqrt{\pi}} E_f \sqrt{A} \qquad \text{(S1)}$$

where A is the contact area at a given depth based on the geometry of the pyramidal Berkovich indenter tip used and β is a correction factor between 1 and 1.058.[6] For the tip used in our study, β = 1.058. The elastic modulus of the perovskites can then be calculated using the Poisson ratio,

σ, with Equation S3:

$$E_f = \frac{1-\sigma^2}{E} + \frac{1-\sigma_{tip}^2}{E_{tip}} \quad \text{(S2).}$$

The nanoindentation results for all five perovskites are provided in Table S2 below. The perovskites with a lighter halide are stiffer while the trend in the elastic modulus for the different cation groups is not immediately obvious. Our elastic modulus values however are in good agreement with available experimental and theoretical literature results.[7,8] The increase of *E* across the $MAPbX_3$ series as X = I < Br < Cl results from size of the halide. As the radius of halide decreases the electronegativity increases, and consequently the packing density of the perovskite lattice, the strength of the Pb–X bonds, and the strength of the hydrogen bonding interactions all increase as well.[7]

V. Calculation of longitudinal and transverse sound speeds

We estimate the average sound speed, $\bar{v}_s$, from the measured *E* by first approximating the longitudinal (v_L) and transverse (v_T) sound speeds with Equations S3 and S4 respectively,[9]

$$v_L = \sqrt{\frac{E}{\rho}\left(\frac{1-\sigma}{(1+\sigma)(1-\sigma)}\right)} \quad \text{(S3)}$$

$$v_T = \sqrt{\frac{E}{2\rho(1+\sigma)}} \quad \text{(S4)}$$

where Poisson ratios range from $0.2 < \sigma < 0.35$. The average sound speed ($\bar{v}_s$) was obtained by combining the longitudinal and transverse velocities:

$$\bar{v}_s = \frac{(v_L+2v_T)}{3} \quad \text{(S5).}$$

The nominal average sound speed was calculated based on the DFT-derived values Poisson ratio of 0.33 (except for $MAPbBr_3$ at 0.29).[10] The values of $\bar{v}_s$ for $MAPbX_3$ differ by at most 18% from prior experimental reports[7,8] and follow the trends in *E* discussed above.

Table S.2: MECHANICAL PROPERTIES OF $APbX_3$ AT ROOM TEMPERATURE*

Perovskite	*E* (GPa)	v_L (m/s)	v_T (m/s)	$\bar{v}_s$ (m/s)
$MAPbCl_3$	23.0 ± 0.72	3278	1651	2194^{+71}_{-108}
$MAPbBr_3$	17.8 ± 1.12	2467	1341	1717^{+126}_{-79}
$MAPbI_3$	12.0 ± 0.33	2078	1047	1390^{+43}_{-66}
$CsPbBr_3$	13.5 ± 1.01	2034	1024	1361^{+74}_{-96}
$FAPbBr_3$	10.2 ± 0.43	1992	1004	1333^{+51}_{-73}

*The nominal sound speeds were calculated using the Poisson ratio of 0.33 (except for $MAPbBr_3$ at 0.29). The uncertainty in the average sound speed was derived using the upper and lower bound in the elastic modulus and a Poisson ratio between 0.35 and 0.2.

VI. Modelling Phonon Dispersion

To model the acoustic phonon dispersion in the lead halide perovskites, two approaches were compared in this paper. Both approaches assume an isotropic Brillouin zone. The first approach uses the linear Debye dispersion with the sound speed ($\bar{v}_s$) and primitive cell number density (η).[11] The second approach implements the Born von Karmen sine-like dispersion,[12,13] using $\bar{v}_s$ values based on our nano-indentation experiments and $\eta = \eta_{\text{cubic}}$ as justified in the paper. Due to the isotropic assumption the maximum wave vector (κ) for both models is defined as $\kappa_{\text{max}} = (6\pi^2\eta)^{1/3}$, which ensures that the isotropic Brillouin zone contains the same number of phonon modes as the real Brillouin zone.[14]

Figure S3 compares the Debye and BvK dispersions with the experimental data from Beecher *et al.* for the acoustic phonons along the Γ-X direction.[15] The BvK model agrees well with the data, while the Debye model based on $\eta = \eta_{\text{cubic}}/4$ and v_s = 4000 m/s is inconsistent with the experimental data.

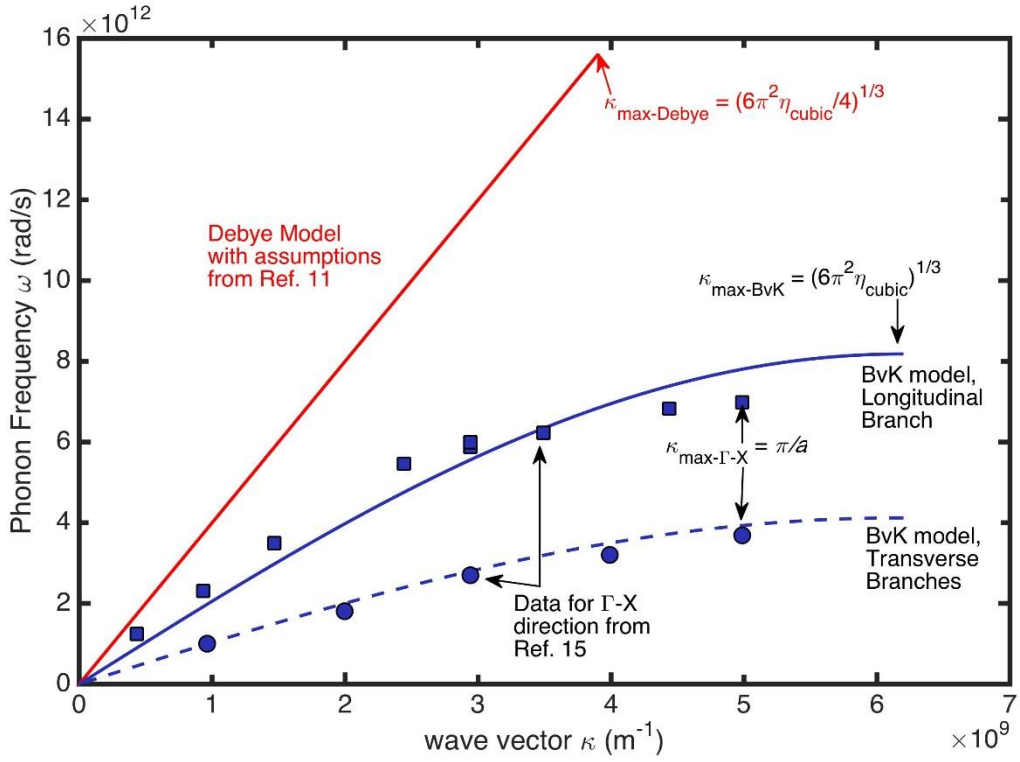

Figure S3: Comparison of the phonon dispersions predicted by the Debye and BvK dispersions with the experimental data from Beecher et al. for the Γ-X direction.[15]

VII. Modelling Thermal Conductivity Accumulation

The thermal conductivity accumulation functions (k_{accum}) are obtained using a modified Callaway model with either the Debye or the Born von Karmen dispersion.[12,13] In both models, the relaxation times (τ) due to the various scattering mechanisms are combined using Matthiessen Rule, $\tau^{-1} = \tau_b^{-1} + \tau_p^{-1} + \tau_u^{-1}$ where $\tau_b^{-1} = v_g / L$ is due to boundary scattering, $\tau_p^{-1} = A\omega^4$ is due to defect scattering, and $\tau_u^{-1} = B\omega^2$ is due to Umklapp scattering, where L is the sample size and A and B are material specific temperature dependent coefficients. An additional term can be added for resonant scattering, $\tau_r^{-1} = D\omega_0^2\omega^2 \Big/ \left(\omega_0^2 - \omega^2\right)^2$ where ω_0 is the resonant scattering frequency and D is a material specific coefficient. The mean free path is given as $\Lambda = v_g\tau$. Values of the coefficients used to create the k_{accum} in Figure 3 for our measured values of thermal conductivity are listed in the tables below. For Debye, we consider impurity scattering with identical A values as in Ref. 11 and fit our measured thermal conductivity for the B value, while for Debye w/ Resonant we considered resonant scattering with the identical D and ω_0 values as in Ref. 11 and fit our measured thermal conductivity for the B value.

Table S.3: Parameters used for Figure 3a ($MAPbI_3$)

	v_s (m/s)	η (nm^{-3})	A (s^3)	B at T= 300 K (s)	ω_0 (rad/s)	D (s^{-1})
Debye	4000	1.0	0.53×10^{-41}	0.76×10^{-14}	–	–
Debye w/ Resonant	4000	1.0	–	0.42×10^{-14}	5.5×10^{12}	1.88×10^{11}
BvK	1390	4.0	–	0.71×10^{-14}	–	–

Table S.4: Parameters used for Figure 3b

Crystal	$\bar{v}_s$ (m/s)	η (nm^{-3})	B at T= 300 K (s)
$MAPbCl_3$	2194	5.53	0.37×10^{-14}
$MAPbBr_3$	1717	4.82	0.50×10^{-14}
$MAPbI_3$	1390	4.0	0.71×10^{-14}
$CsPbBr_3$	1361	5.02	0.57×10^{-14}
$FAPbBr_3$	1333	4.66	0.52×10^{-14}

VIII. References

(1) Glaser, T.; Müller, C.; Sendner, M.; Krekeler, C.; Semonin, O. E.; Hull, T. D.; Yaffe, O.; Owen, J. S.; Kowalsky, W.; Pucci, A.; Lovrinčić, R. *J. Phys. Chem. Lett.* **2015**, *6*, 2913–2918.

(2) Semonin, O. E.; Elbaz, G. A.; Straus, D. B.; Hull, T. D.; Paley, D. W.; van der Zande, A. M.; Hone, J. C.; Kymissis, I.; Kagan, C. R.; Roy, X.; Owen, J. S. *J. Phys. Chem. Lett.* **2016**, *7*, 3510–3518.

(3) Elbaz, G. A.; Straus, D. B.; Semonin, O. E.; Hull, T. D.; Paley, D. W.; Kim, P.; Owen, J. S.; Kagan, C. R.; Roy, X. *Nano Lett.* **2017**, *17*, 1727–1732.

(4) Furukawa, G. T.; Saba, W. G.; Reilly, M. L. *Critical analysis of the heat-capacity data of the literature and evaluation of thermodynamic properties of copper, silver, and gold, from 0 to 300 K*; U.S. Dept. of Commerce, National Bureau of Standards: Washington, D.C., 1968.

(5) Knop, O.; Wasylishen, R. E.; White, M. A.; Cameron, T. S.; Oort, M. J. M. Van. *Can. J. Chem.* **1990**, *68*, 412–422.

(6) Tsui, T. Y.; Pharr, G. M. *J. Mater. Res.* **1999**, *14*, 292–301.

(7) Rakita, Y.; Cohen, S. R.; Kedem, N. K.; Hodes, G.; Cahen, D. *MRS Commun.* **2015**, *5*, 623–629.

(8) Sun, S.; Fang, Y.; Kieslich, G.; White, T. J.; Cheetham, A. K. *J. Mater. Chem. A* **2015**, *3*, 18450–18455.

(9) Kinsler, L. E.; Frey, A. R.; Coppens, A. B.; Sanders, J. V. *Fundamentals of acoustics*; 4th ed.; Wiley, 1999.

(10) Feng, J. *APL Mater.* **2014**, *2*, 81801.

(11) Pisoni, A.; Jaćimović, J.; Barišić, O. S.; Spina, M.; Gaál, R.; Forró, L.; Horváth, E. *J. Phys. Chem. Lett.* **2014**, *5*, 2488–2492.

(12) Yang, F.; Dames, C. *Phys. Rev. B* **2013**, *87*, 35437.

(13) Chen, G.; Dames, C. In *Thermoelectrics Handbook*; CRC Press, 2005; pp. 42-1-42–16.

(14) Kittel, C. *Introduction to solid state physics*; 8th ed.; John Wiley & Sons, Ltd: Hoboken, NJ, 2005.

(15) Beecher, A. N.; Semonin, O. E.; Skelton, J. M.; Frost, J. M.; Terban, M. W.; Zhai, H.; Alatas, A.; Owen, J. S.; Walsh, A.; Billinge, S. J. L. *ACS Energy Lett.* **2016**, *1*, 880–887.